

A neutron diffraction study of structural and magnetic transformations in $A\text{FeO}_2$ ($A = \text{K}, \text{Rb}$ and Cs)

This article has been downloaded from IOPscience. Please scroll down to see the full text article.

2010 J. Phys.: Condens. Matter 22 426001

(<http://iopscience.iop.org/0953-8984/22/42/426001>)

View [the table of contents for this issue](#), or go to the [journal homepage](#) for more

Download details:

IP Address: 192.33.126.162

The article was downloaded on 02/12/2010 at 10:31

Please note that [terms and conditions apply](#).

A neutron diffraction study of structural and magnetic transformations in $A\text{FeO}_2$ ($A = \text{K}, \text{Rb}$ and Cs)

D Sheptyakov¹, N Z Ali² and M Jansen²

¹ Laboratory for Neutron Scattering, Paul Scherrer Institut, CH-5232 Villigen PSI, Switzerland

² Max-Planck-Institut für Festkörperforschung, Heisenbergstraße 1, D-70569 Stuttgart, Germany

E-mail: denis.cheptiakov@psi.ch

Received 1 July 2010, in final form 9 September 2010

Published 4 October 2010

Online at stacks.iop.org/JPhysCM/22/426001

Abstract

In continuation of our recent x-ray study of the structural phase transitions in the $A\text{FeO}_2$ ($A = \text{K}, \text{Rb}, \text{Cs}$) family, we have systematically investigated the respective structural and magnetic phase transitions by neutron powder diffraction. While the temperatures of the first-order structural phase transitions are strongly different for the three compounds (~ 1003 , ~ 737 and ~ 350 K for $A = \text{K}, \text{Rb}, \text{Cs}$) and systematically decrease with increasing ionic radius of the A-cation, the magnetic transition temperatures in all three compounds have been found to be almost the same—slightly above 1000 K. The magnetic ordering type is similar in all three compounds—antiferromagnetic ordering of magnetic Fe^{3+} ions within the system of the three-dimensional Fe–O–Fe linkages such that the Fe–Fe exchange between the nearest neighboring ions is always antiferromagnetic. The directions of magnetic Fe moments were found to be parallel to the crystallographic axis c in RbFeO_2 and CsFeO_2 and parallel to the axis b in KFeO_2 in notations of their low-temperature orthorhombic modifications.

(Some figures in this article are in colour only in the electronic version)

1. Introduction

The alkali metal oxoferrates (III) $A\text{FeO}_2$ ($A = \text{K}, \text{Rb}$ and Cs) are isostructural and belong to the structure family of stuffed cristobalites. As a common feature, these structures display a three-dimensional network of corner sharing tetrahedra, $\text{FeO}_{4/2}$, providing space for including further cations for the sake of charge compensation. Since the tetrahedral framework can easily undergo collective tilting motions, it is adaptable to accommodate cations of various sizes. This flexibility, however, introduces a complex variety of static and dynamic disorder, and the above mentioned ferrates are particularly well suited for studying the related structural order–disorder transitions in comparison [1]. All of the three ferrates show static disorder at low temperatures, frozen in by twinning, and a transition to dynamically disordered polymorphs of average cubic symmetry at rising temperature [2]. The tilting Fe–O–Fe angles and the transition temperatures vary systematically with the size of the alkali ions. From such structural features

one would deduce strong, non-frustrated antiferromagnetic ordering, which, however, is expected to be modulated by the systematic variations in the Fe–O–Fe angles as caused by the countercations, and possibly by the librational degrees of freedom. Thus, the title compounds appear to be an appropriate reference system for studying interrelations between structural and magnetic order–disorder transitions.

The magnetic phase transition in KFeO_2 was first observed by Mössbauer effect measurements in 1970 [3], where its extremely high Néel temperature of 988 ± 10 K was for the first time established, and then by neutron powder diffraction in 1977 [4]. In the same work [4], the existence of the structural phase transformation near the Néel temperature (deduced to be 960 ± 10 K) has been noticed. In the present paper, we extend this investigation to the study of the magnetic ordering phenomena for the whole family of respective potassium, rubidium and cesium ferrates. By neutron powder diffraction, we determine the magnetic structures in all three compounds to be antiferromagnetic, with the Néel temperatures of slightly

above 1000 K being very similar in all of them and only weakly increasing when going from $A = \text{K}$ to Rb and Cs .

2. Experimental details

2.1. Sample preparation and characterization

A total of about 4 g of polycrystalline samples of the respective AFeO_2 compounds were prepared in several batches along the ‘azide nitrate route’ [5], under argon stream as described in our earlier publication [2]. Each batch was checked with x-ray diffraction to confirm its purity as a single phase. The samples were sealed inside cylindrical vanadium containers of 6 mm diameter for neutron studies.

2.2. Diffraction experiments

The neutron diffraction data were collected at the neutron powder diffractometer HRPT [6] with the neutron wavelength $\lambda = 1.886 \text{ \AA}$, using the closed-cycle refrigerator for the low temperature ($10 \dots 300 \text{ K}$) and evacuated radiation-type furnace for the high-temperature (up to 1080, 1030 and 1100 K for $A = \text{K}$, Rb and Cs , respectively) measurements. All the measurements were carried out on heating the samples from low to high temperatures. We used the advantage of the previously carried out synchrotron x-ray diffraction experiments reported in [2] on exactly the same samples, although, unlike in the synchrotron x-ray diffraction measurements, we have managed to avoid any decomposition of the samples upon heating. The necessity for the use of both synchrotron x-ray and neutron diffraction was two-fold. On the one hand, we needed the high resolution of the synchrotron data in order to precisely monitor the structural parameters in the proximity of the phase transitions, where the splitting of diffraction lines due to the orthorhombic distortions becomes really tiny. On the other hand, we intended to tackle the correlations between the magnetic ordering and the crystal structure in the title compounds, in particular the details of the oxygen site disorder at the structural transition points, thus the use of neutron diffraction for simultaneous crystal and magnetic structure study became indispensable.

The symmetry analysis of the possible magnetic structures has been carried out with the program SARAH-2k [7], and the refinements of the parameters of both the crystal and magnetic structure parameters were done with the Fullprof suite of programs [8] using its internal scattering lengths and magnetic scattering form-factors for the Fe^{3+} ion.

3. Results

3.1. Structural phase transitions, crystal structures of the low-temperature and high-temperature modifications

As already known [4], KFeO_2 undergoes a structural phase transition near its Néel temperature such that (citing directly [4]) ‘The structure above T_N should be more regular’. In our recent study of the structural phase transitions [2], in agreement with the previous findings, we have observed a structural phase transition at $\sim 1003 \text{ K}$ (in KFeO_2), and

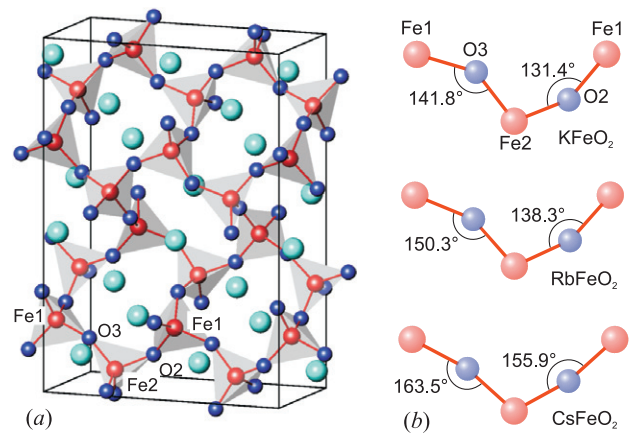


Figure 1. (a) Schematic representation of the crystal structures of AFeO_2 ($A = \text{K}$, Rb and Cs) near room temperature (crystal structure of RbFeO_2 at 300 K). The Fe atoms are shown as red tetrahedra centers, the coordinating O atoms as blue, and the Rb atoms as cyan spheres. (b) Illustration of the systematic increase of the Fe–O–Fe angles with increasing size of the A-cations. The Fe1–O3–Fe2–O2–Fe1 chain (also marked in panel (a)) as viewed in the direction perpendicular to the plane containing the three Fe atoms.

additionally—similar transitions at $\sim 737 \text{ K}$ (for RbFeO_2), and at $\sim 350 \text{ K}$ (for CsFeO_2).

The temperature evolutions of the crystal and magnetic structures of KFeO_2 , RbFeO_2 and CsFeO_2 have been precisely investigated in the present study by neutron powder diffraction. In their room temperature modifications and also at lower temperatures down to $T = 10 \text{ K}$, all the three ferrates are isostructural to orthorhombic KGaO_2 [9–11] (space symmetry $Pbca$), with lattice constants e.g. for KFeO_2 (at room temperature) $a \approx 5.600 \text{ \AA}$, $b \approx 11.26 \text{ \AA}$, $c \approx 15.94 \text{ \AA}$, thus interrelated as

$$a \approx \frac{b}{2} \approx \frac{c}{2\sqrt{2}}.$$

The crystal structure parameters of all three compounds have been refined from the neutron powder diffraction data, and are listed in table 1.

In figure 1(a), we represent the schematic drawing of the room temperature crystal structures of the title AFeO_2 compounds; the crystal structure of RbFeO_2 at $T = 300 \text{ K}$ has been taken for illustration. The interatomic Fe–O distances are very similar in all three structures and amount on average to 1.86 \AA . However, when going from KFeO_2 to RbFeO_2 and to CsFeO_2 , the unit cell volumes increase with the respective sizes of the alkali cations: from ~ 1005 to ~ 1076 to $\sim 1180 \text{ \AA}^3$. This gain in volume in order to accommodate the alkali metal cations of correspondingly bigger sizes is achieved by increasing of the Fe–O–Fe bond angles. They amount at room temperature on average to 137° , 143° and 157° for KFeO_2 , RbFeO_2 and CsFeO_2 , respectively. Thus, in the compound with the largest A-cation (in CsFeO_2), the Fe–O–Fe connections are much more ‘straight’ than in RbFeO_2 and in KFeO_2 , in which they are the most bent. This systematic increase of the Fe–O–Fe angles is illustrated in figure 1(b).

Table 1. Crystal structure parameters at about room temperature for the AFeO₂ (A = K, Rb and Cs) compounds refined from neutron powder diffraction data. Space group *Pbca* (*Z* = 16). All atoms are located in the general (8c) sites.

Parameter		KFeO ₂ (320 K)	RbFeO ₂ (300 K)	CsFeO ₂ (306 K)
<i>a</i> (Å)		5.6002 (1)	5.7197 (1)	5.9167 (1)
<i>b</i> (Å)		11.2602 (2)	11.5141 (2)	11.8860 (2)
<i>c</i> (Å)		15.9414 (2)	16.3457 (2)	16.7792 (3)
<i>V</i> (Å ³)		1005.25 (3)	1076.49 (3)	1180.01(3)
A1 (K, Rb, Cs)	<i>x</i>	0.745 (2)	0.749 (1)	0.747 (2)
	<i>y</i>	0.5095 (10)	0.5105 (5)	0.5023 (10)
	<i>z</i>	0.4357 (11)	0.4371 (5)	0.4374 (10)
A2 (K, Rb, Cs)	<i>x</i>	0.3039 (14)	0.3009 (7)	0.2888 (11)
	<i>y</i>	0.2370 (11)	0.2390 (4)	0.2452 (9)
	<i>z</i>	0.684 (1)	0.6866 (4)	0.6870 (9)
A1, A2	<i>B</i> (Å ²)	1.76 (10)	1.65 (4)	1.89 (6)
Fe1	<i>x</i>	0.7537 (7)	0.7554 (5)	0.7513 (9)
	<i>y</i>	0.0084 (4)	0.0056 (3)	0.0022 (5)
	<i>z</i>	0.1884 (4)	0.1900 (3)	0.1884 (6)
Fe2	<i>x</i>	0.7842 (5)	0.7842 (4)	0.7726 (5)
	<i>y</i>	0.2352 (3)	0.2396 (3)	0.2459 (5)
	<i>z</i>	0.5648 (4)	0.5631 (3)	0.5636 (5)
Fe1, Fe2	<i>B</i> (Å ²)	0.85 (33)	0.55 (3)	0.89 (3)
O1	<i>x</i>	0.4325 (14)	0.4431 (10)	0.4628 (17)
	<i>y</i>	0.9805 (7)	0.9825 (5)	0.9907 (8)
	<i>z</i>	0.2179 (5)	0.2208 (4)	0.2317 (7)
O2	<i>x</i>	0.8411 (14)	0.8285 (11)	0.7924 (17)
	<i>y</i>	0.9082 (8)	0.9022 (5)	0.8880 (10)
	<i>z</i>	0.1008 (5)	0.1058 (4)	0.1146 (6)
O3	<i>x</i>	0.7985 (14)	0.8028 (12)	0.7832 (16)
	<i>y</i>	0.1649 (7)	0.1551 (5)	0.1389 (12)
	<i>z</i>	0.1573 (5)	0.1484 (4)	0.1377 (6)
O4	<i>x</i>	0.5774 (15)	0.5766 (10)	0.5569 (13)
	<i>y</i>	0.2934 (7)	0.2836 (6)	0.2711 (8)
	<i>z</i>	0.4804 (4)	0.4805 (3)	0.4841 (5)
O 1...4	<i>B</i> (Å ²)	1.92 (6)	1.30 (5)	1.87 (5)

The Fe1–O3–Fe2–O2–Fe1 chain contains the largest (Fe1–O3–Fe2) and the smallest (Fe2–O2–Fe1) among all the Fe–O–Fe angles in the structure. The direction of view in figure 1(b) is perpendicular to the plane containing the three Fe atoms. On the other hand, the interatomic Fe–Fe separations through these bonding are the smallest in KFeO₂ (3.45 Å on average), intermediate in RbFeO₂ (3.53 Å on average) and the largest in CsFeO₂ (3.63 Å on average). Both these Fe–Fe bond lengths and the Fe–O–Fe bond angles determine the strengths of the magnetic exchange couplings between the Fe³⁺ ions: the more ‘straight’ the Fe–O–Fe junction and the ‘shorter’ the Fe–Fe interatomic separation are, the stronger is the exchange. As we will see later, these two effects ‘compensate’ each other in such a way that, effectively, the magnetic exchange energies and the magnetic transition temperatures in all three compounds are very similar to each other.

The high-temperature modifications of all three compounds (emerging at different temperatures) have been found to also be isostructural to each other. All the diffraction patterns of the high-temperature modifications of KFeO₂, RbFeO₂ and CsFeO₂ have been indexed on a cubic F-centered unit cell with a lattice constant a_{cub} related to those of the corresponding orthorhombic low-temperature modifications as:

$$a_{\text{cub}} \approx a_{\text{orth}}\sqrt{2} \approx \frac{b_{\text{orth}}}{\sqrt{2}} \approx \frac{c_{\text{orth}}}{2}.$$

In extension to our previous work [2] which was based solely on the x-ray diffraction data, in the current neutron study we were able to extract more precise information on the details of the high-temperature modifications of the title compounds. In particular, in [2], based only on the synchrotron x-ray diffraction data, we were treating displacements of the oxygen atoms in the high-temperature modifications of the AFeO₂ compounds with the anisotropic thermal parameters. Having now the neutron data at hand, we are able to get a deeper insight into the mechanism of the structural phase transition into a cubic phase in the studied compounds. Previously we were assuming [2] that upon heating the samples the bridging oxygen atoms forming the bent Fe–O–Fe junctions become disordered in the plane perpendicular to the Fe–Fe direct linkage, such that the Fe–O–Fe bonds become apparently straight, producing an average Fe–O–Fe angle of 180° (figure 2, panels (a) and (b)). In reality, however, it is just long-range three-dimensional order of the precise mutual orientations of the still effectively bent Fe–O–Fe linkages which become lost in the transition. Thus, because of this dynamical disorder of the long-range correlations in the mutual directions of the Fe–O–Fe linkages, oxygen (speaking in terms of crystallographic description) becomes disordered on a ring perpendicular to the Fe–Fe bond, as illustrated in figure 2, panel (c).

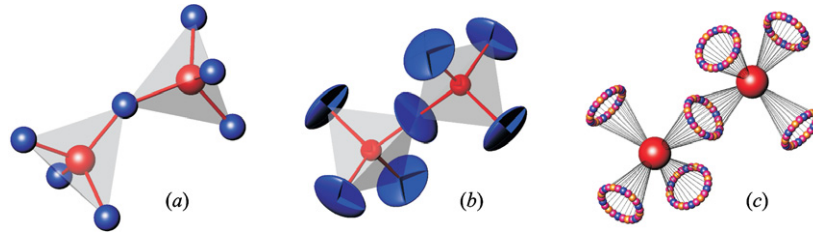


Figure 2. Illustration of the crystal structure peculiarities of RbFeO₂ associated with the structural transition. (a) Fe1–O–Fe2 junction at $T = 300$ K, in the orthorhombic ordered phase (b) Fe–O–Fe junction in the high-temperature phase ($T = 820$ K); approach with the anisotropic thermal parameters for the oxygen atoms used in our work [2], (c) same, the newly proposed approach based on split oxygen sites. The Fe atoms are shown as red spheres, the O atoms as blue spheres or ellipsoids in the panels (a) and (b), or as the multicolored tiny spheres forming rings in panel (c).

In order to most properly model this structural peculiarity of the high-temperature phases of the AFeO₂ ($A = \text{K, Rb and Cs}$) compounds, we assumed the bridging oxygen atoms to be disordered on a circle with a radius R perpendicular to the Fe–Fe junction. Thus, instead of occupying the 16c (0, 0, 0) position, each oxygen is split into 24 equally occupied and equally spaced along the circle ‘atoms’ occupying three sites: O1 in the 96h ($-x_1, 0, x_1$), O2 in the 96g ($-x_2, -x_2, 2x_2$) and O3 in the 192i ($-x_3, -y_3, x_3 + y_3$). In order to keep the ring really uniform, the coordinates for these sites are forced in our refinements to be related to the radius R of the ring and the cubic lattice constant a_{cub} as follows:

$$\begin{aligned} x_1 &= \frac{1}{\sqrt{2}} \frac{R}{a_{\text{cub}}} & x_2 &= \frac{1}{\sqrt{6}} \frac{R}{a_{\text{cub}}} & x_3 &= \frac{1}{\sqrt{3}} \frac{R}{a_{\text{cub}}}; \\ y_3 &= \sqrt{\frac{2 - \sqrt{3}}{6}} \frac{R}{a_{\text{cub}}}. \end{aligned} \quad (1)$$

The occupation factors for the O1, O2 and O3 sites are exactly 1/24. This way, the angular span between the neighboring individual O_i ($i = 1-3$) atoms along the ring is exactly 15°. This approach allows us to realistically model the true temperature dependences of the interatomic distances and angles in the studied compounds. Notably, taking this measure does not require the number of the refined structural parameters to increase. Instead of the two components of the anisotropic thermal parameter tensor ($\beta_{11} = \beta_{22} = \beta_{33}$ and $\beta_{12} = \beta_{13} = \beta_{23}$ of the oxygen atom located in (0, 0, 0)) [2], we are now refining another two parameters: R (by properly constraining the values of x_1, x_2, x_3 and y_3 : see equations (1)) and the isotropic thermal parameters $B_{\text{iso}}(\text{O})$ constrained to be identical for the atoms O1, O2 and O3. The agreement factors of the refinement indeed become significantly better with such a new model, for example for the case of the RbFeO₂ data collected at $T = 820$ K, the χ^2 improves from 2.01 to 1.77, the Bragg R -factor for the crystallographic RbFeO₂ phase from 5.51% to 4.14%, and the magnetic R -factor for the RbFeO₂ antiferromagnetic phase from 11.0% to 7.8%. The refined values of the structural parameters in the cubic phases of all three compounds are presented in table 2 for selected representative temperatures (different for each compound).

In figure 3, the illustration of the crystal structures of the high-temperature crystallographic phases of the AFeO₂

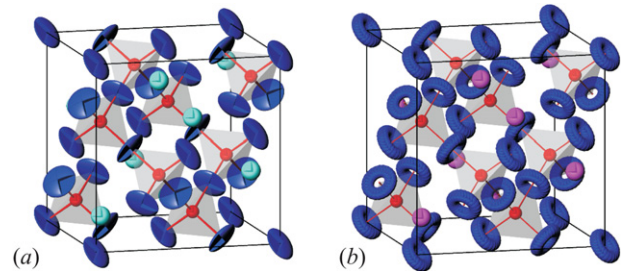


Figure 3. Crystal structures of the high-temperature modifications of KFeO₂, RbFeO₂ and CsFeO₂. (a) From the model with the anisotropic thermal parameters for oxygen atoms as in [2], (b) approach of the current work with oxygen atoms being disordered on a ring. The sizes of the atoms are proportional to the refined thermal parameters of the atoms in RbFeO₂ at $T = 820$ K.

($A = \text{K, Rb and Cs}$) compounds is given, with the strongly anisotropic character of the atomic thermal vibrations of the oxygen atoms (a) [2], and in the split atom model of the present work (b). In panel (b) of figure 3, the FeO₄ tetrahedra are displayed with the Fe–O linkages based on the ‘time-average’ positions of the corresponding oxygen atoms, though in reality, the oxygen atomic density is of course evenly distributed on the corresponding rings perpendicular to the Fe–Fe directions. Thus upon heating, as soon as the temperature-induced increase in the atomic displacement parameters (ADPs) of oxygen atoms is large enough, the oxygen atoms ‘jump’ in a quantum-like manner from a given position with a well-defined orientation of the Fe–O–Fe bond angle into the state illustrated in figure 3(b), where these angles are of course preserved, but their orientations vary dynamically in a collective manner.

The structural phase transitions in all three compounds are of the first order, which has been convincingly illustrated by the unit cell volume discontinuities at the phase transitions, by the presence of certain temperature ranges of coexistence of the low- and high-temperature modifications, and by the temperature hysteresis of the transitions seen clearly in the DSC measurements [2]. In agreement with these previous findings, here we also observe the unit cell volume discontinuities at the phase transitions, as illustrated in figure 4. The temperature steps during the neutron data collection were however too coarse to be able to track in detail the coexistence of the two phases in the given temperature intervals.

Table 2. Crystal structure parameters for the high-temperature polymorphs of KFeO_2 (at $T \approx 1050$ K), RbFeO_2 (at $T \approx 820$ K) and CsFeO_2 (at $T \approx 400$ K) refined from neutron powder diffraction data. Space group $Fd\bar{3}m$ ($Z = 8$). Atoms A (K, Rb, Cs) at 8b sites ($3/8, 3/8, 3/8$), Fe at 8a sites ($1/8, 1/8, 1/8$), O1 at 96h ($-x_1, 0, x_1$), O2 at 96g ($-x_2, -x_2, 2x_2$) and O3 at 192i ($-x_3, -y_3, x_3 + y_3$) sites. The x_1, x_2, x_3 and y_3 positional parameters are correlated to essentially one parameter—the radius of the ring R according to the expressions (1). The fractional occupation factors for the O1, O2 and O3 are all equal to $1/24$.

Parameter		KFeO_2 (1050 K)	RbFeO_2 (820 K)	CsFeO_2 (400 K)
a (Å)		8.091 71 (9)	8.242 63 (6)	8.411 03 (4)
A (K, Rb, Cs)	B (Å ²)	7.57 (15)	5.40 (7)	2.84 (5)
Fe	B (Å ²)	3.64 (5)	2.47 (3)	1.27 (3)
O(1, 2, 3)	R (Å)	0.638 (3)	0.533 (3)	0.385 (3)
O(1, 2, 3)	B (Å ²)	4.40 (15)	2.35 (11)	1.33 (9)
Fe–O	Distance (Å)	1.865 (2)	1.8624 (14)	1.8611 (14)
Fe–O–Fe	Angle (deg)	139.95 (9)	146.76 (6)	156.17 (6)

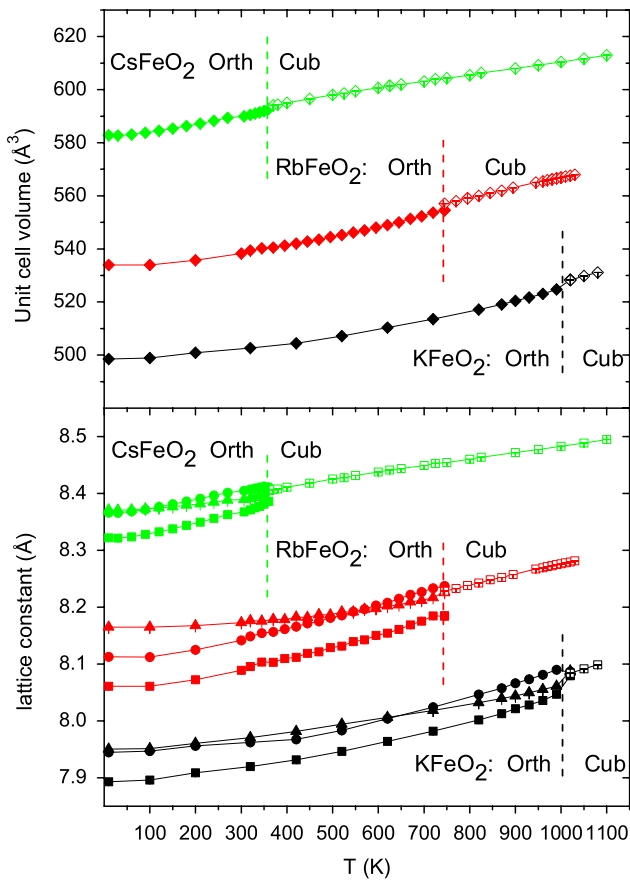


Figure 4. Temperature dependences of the refined unit cell parameters (\blacksquare — $a_{\text{orth}}\sqrt{2}$, \bullet — $b_{\text{orth}}/\sqrt{2}$, \blacktriangle — $c_{\text{orth}}/2$ for the orthorhombic phases, \square — a_{cub} for the cubic phases) and of the unit cell volumes (\blacklozenge — $V_{\text{orth}}/2$, \blacklozenge — V_{cub}) of the orthorhombic low-temperature and cubic high-temperature crystallographic modifications of the AFeO_2 ($A = \text{K, Rb}$ and Cs) compounds. The transition temperatures are also indicated.

We observe that the discontinuities of the unit cell volumes at the structural transition temperatures are of the order of $\sim 3 \times 10^{-3}$.

The newly evolved structural model for the high-temperature modifications of the AFeO_2 ($A = \text{K, Rb}$ and Cs) compounds allows also for a more realistic quantification of the internal structural changes with temperature.

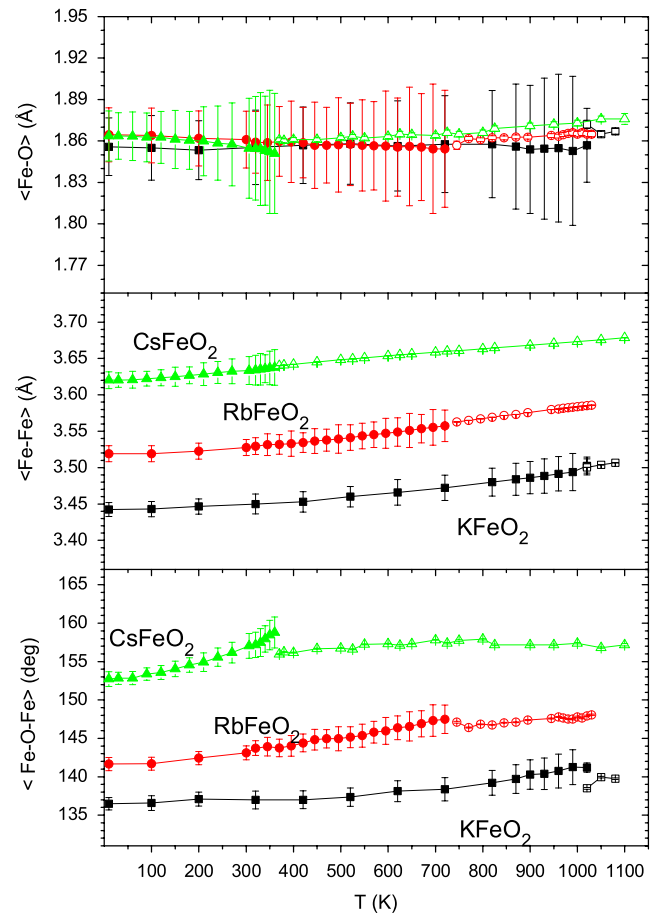


Figure 5. Temperature dependences of the average interatomic Fe–O (top), Fe–Fe (middle) distances and of the average Fe–O–Fe bond angle (bottom) in the AFeO_2 compounds (\blacksquare and \square —for KFeO_2 , \bullet and \circ —for RbFeO_2 , \blacktriangle and \triangle —for CsFeO_2). Filled and opened symbols represent the results for the low-temperature orthorhombic and for the high-temperature cubic phases respectively.

From figure 5, it is seen that the Fe–O bond distances are practically temperature-independent in the whole temperature range up to ~ 1100 K and also are essentially identical in all three compounds. They amount on average to 1.86 Å, and display very slight discontinuities of ~ 0.01 Å at the structural transition temperatures. In contrast, the Fe–O–Fe bond angles strongly increase with temperature (much

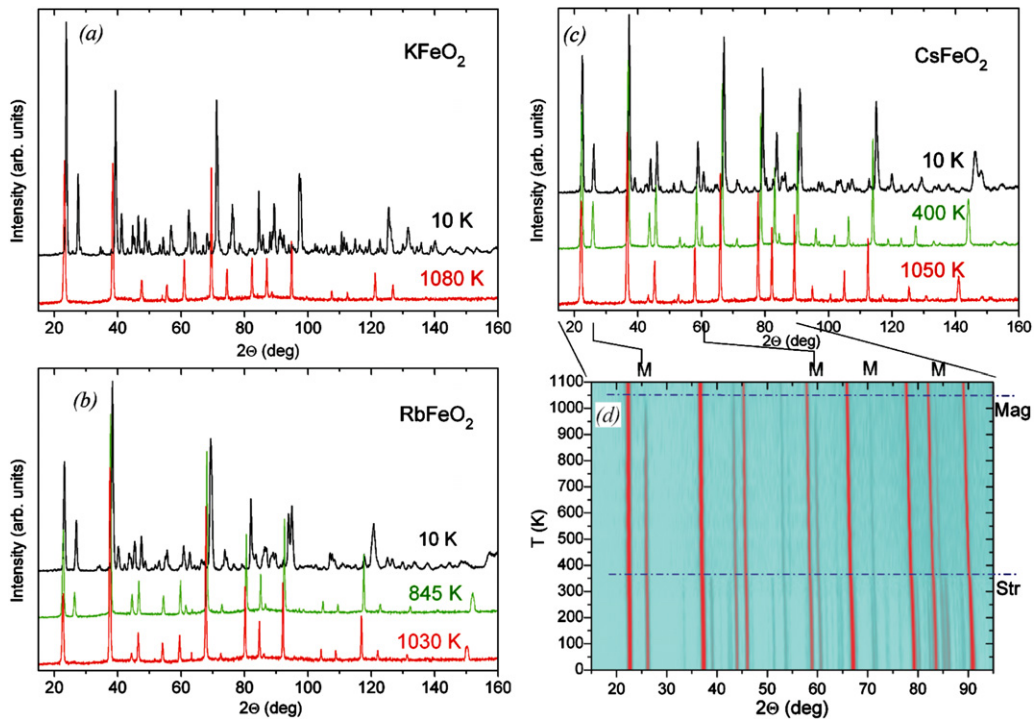


Figure 6. (a) Neutron powder diffraction (NPD) patterns of the KFeO₂ compound recorded for the orthorhombic and magnetic LT phase at $T = 10$ K and for the cubic and paramagnetic HT phase at 1080 K; (b) NPD patterns of the RbFeO₂ compound recorded for the orthorhombic and magnetic LT phase at $T = 10$ K, for the cubic and still magnetic HT phase at $T = 845$ K; and for the cubic and paramagnetic HT phase at $T = 1030$ K; (c) NPD patterns of the CsFeO₂ compound recorded for the orthorhombic and magnetic LT phase at $T = 10$ K, for the cubic and still magnetic HT phase at $T = 400$ K; and for the cubic and paramagnetic HT phase at $T = 1050$ K; (d) color intensity map of the temperature evolution of the diffraction patterns of CsFeO₂ (fragments of 36 diffraction patterns recorded between 10 and $T = 1100$ K in a 2θ range from 15° to 95°). The horizontal dash-dotted lines indicate the temperatures of the structural (Str) and magnetic (Mag) phase transitions. The most evident magnetic diffraction peaks positions are marked with M.

faster in the orthorhombic phase, followed by visible negative discontinuities at the structural transitions and slower increases in the cubic phase), which leads in turn to the significant increases of the Fe–Fe distances with temperature: by as much as $0.06 \dots 0.07$ Å on heating from low temperatures to ≥ 1000 K.

3.2. Neutron diffraction results. Magnetic transitions. Magnetic structures

In the neutron diffraction patterns of all three AFeO₂ ($A = \text{K, Rb and Cs}$) compounds recorded at different temperatures, in addition to the structural phase transitions discussed above we also observe magnetic ones. These are related to the long-range magnetic ordering of the spins of the Fe³⁺ ions. An illustration of the observation of these two transitions is given in figure 6: in panels (a) and (b) for KFeO₂ and RbFeO₂ respectively, and in (c) and (d) for CsFeO₂.

The signatures of both the structural phase transition (disappearance of some of the orthorhombic structure diffraction lines) at ~ 370 K and of the magnetic transition at ~ 1055 K are clearly noticeable in case of CsFeO₂. The diffraction peaks at $\sim 26.5^\circ$, $\sim 44^\circ$, $\sim 61^\circ$ etc are of magnetic origin. Qualitatively similar observations have been made for the KFeO₂ and RbFeO₂ compounds as well.

The set of the magnetic diffraction lines in all three AFeO₂ ($A = \text{K, Rb and Cs}$) compounds is indexed in the parent

orthorhombic primitive unit cell, thus the propagation vector of the magnetic structure is $\kappa = [0, 0, 0]$. The symmetry analysis of the possible magnetic structures with this propagation vector for the positions of Fe ions in the unit cell of AFeO₂ ($A = \text{K, Rb and Cs}$) with a space group $Pbca$ has been carried out with the Program SARAh-2k [7], assuming that for both magnetic Fe³⁺ sites the ordering occurs with one and the same irreducible representation (IR). A total of eight IRs, for which the decomposition for both Fe sites has nonzero coefficients, enter the decomposition of the magnetic representation for either of the sites Fe1 and Fe2. All resulting possibilities have been checked by Rietveld refinement, and it has been found that for all three compounds there is exactly one IR providing the ideal fit. These magnetic structures correspond to antiferromagnetic ordering of the magnetic moments at the Fe sites such that the Fe–Fe couplings are antiferromagnetic in all four possible Fe–Fe linkages. Interestingly enough, the direction of the magnetic Fe³⁺ moments have been found to be parallel to the crystallographic b axis for KFeO₂, and to the crystallographic c axis for RbFeO₂ and CsFeO₂. This assignment of the moment directions is rather strict, since choosing the direction of the magnetic moments along the other crystallographic axis (choosing another IR) results in noticeable poisoning of the refinement, manifesting itself in the significant worsening of the refinement agreement factors. For example in the case of the 10 K dataset of CsFeO₂, choosing the direction of the magnetic moments along the

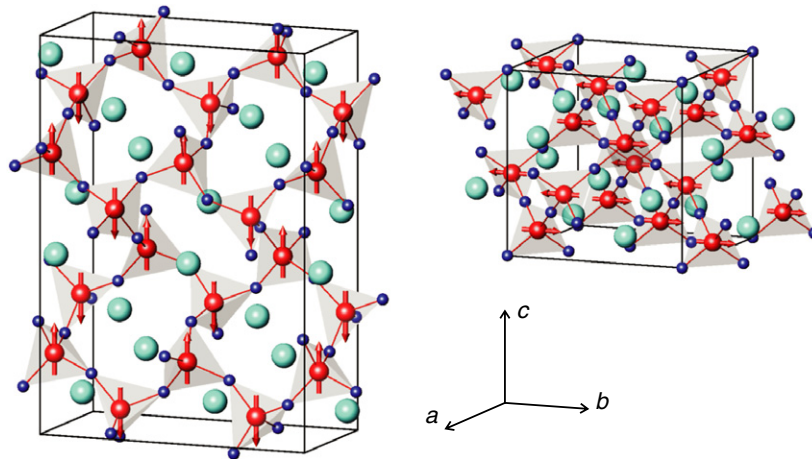


Figure 7. Illustrations of the magnetic structure of RbFeO_2 at $T = 300$ K (in the low-temperature orthorhombic phase, left panel) and at $T = 820$ K (high-temperature cubic phase, right panel).

crystallographic axes a or b instead of c leads to an increase of the magnetic R -factor for the magnetic phase from 2.43% to 3.52% and 3.23%, and of the global weighted χ^2 from 1.45 to 1.75 and 1.61 respectively. Similar judgments are also valid for RbFeO_2 and KFeO_2 with the corresponding moment directions. The magnetic Fe^{3+} moment direction in KFeO_2 contradicts the earlier finding of [4], where the crystallographic axis a direction was proposed as the most probable for KFeO_2 . The determination of the magnetic Fe^{3+} moment directions for RbFeO_2 and for CsFeO_2 has been done here for the first time. Interestingly enough, if one considers the directions of magnetic moments in the orthorhombic low-temperature modifications of the studied compounds, the case of KFeO_2 is physically different from those of both RbFeO_2 and CsFeO_2 . In the former case (KFeO_2), the magnetic Fe moments are aligned parallel to the direction of one of the Fe–O–Fe zig-zag chains and thus parallel to one of the plane diagonals of the parent (high-temperature) cubic unit cell, while in both RbFeO_2 and CsFeO_2 they are perpendicular to this direction (inclined at different angles to the directions of *all* the Fe–O–Fe zig-zag chains), thus formally being aligned along one of the unit cell basic vectors of the parent high-temperature cubic cell. In the high-temperature cubic phases, the magnetic structures stay essentially the same, with the only difference being that all directions (a , b , c) become equal, so we arbitrarily direct the moments in all three compounds along the crystallographic axis a (though, for KFeO_2 , in order to preserve the consistency with the magnetic moment directions in the low-temperature orthorhombic phase, one would rather direct them along any plane diagonal of the cube, e.g. along the $a + b$ direction; we cannot however distinguish these peculiar details in our powder experiment, so all three compounds were just supposed to have the magnetic moments directions along the a lattice direction in the high-temperature cubic form). The illustration of the magnetic structures of the low- and high-temperature modifications of the title AFeO_2 ($A = \text{K}, \text{Rb}$ and Cs) compounds is given in figure 7 for the case of RbFeO_2 .

The quality of the Rietveld refinements of crystal and magnetic structure parameters from neutron powder diffraction

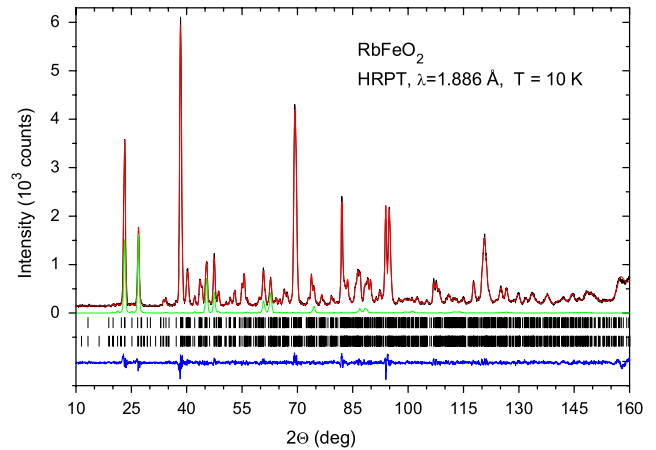


Figure 8. Rietveld refinement fit of RbFeO_2 at $T = 10$ K (low-temperature orthorhombic phase). Experimental points, calculated profile and the difference curve are shown. The ticks below the graph indicate the calculated positions of the diffraction peaks: chemical structure (top) and magnetic phase (bottom). The contribution of solely the magnetic diffraction to the total diffraction intensity is shown in green.

data is demonstrated in figure 8 for the RbFeO_2 refinement at $T = 10$ K.

The magnetic moment magnitudes refined from the neutron powder diffraction data are presented in figure 9. The data in figure 9 were fitted to the empirical equation

$$M(T) = M_0 * \left[1 - \left(\frac{T}{T_N} \right)^{\alpha} \right]^{\beta} \quad (2)$$

which qualitatively fits the data well at all temperatures below T_N . In the limit of low temperatures, $M(T) \sim M_0 * [1 - \beta * (T/T_N)^{\alpha}]$, thus the asymptotic behavior of the model function $M(T)$ is determined by α , while at $T \rightarrow T_N$, $M(T) \sim M_0 * \alpha^{\beta} * [1 - T/T_N]^{\beta}$, so when approaching the T_N , the expression (2) for $M(T)$ is simplified to the usual critical exponent expression, with the asymptotic being determined by β . The refined values of the fitting parameters are summarized in table 3.

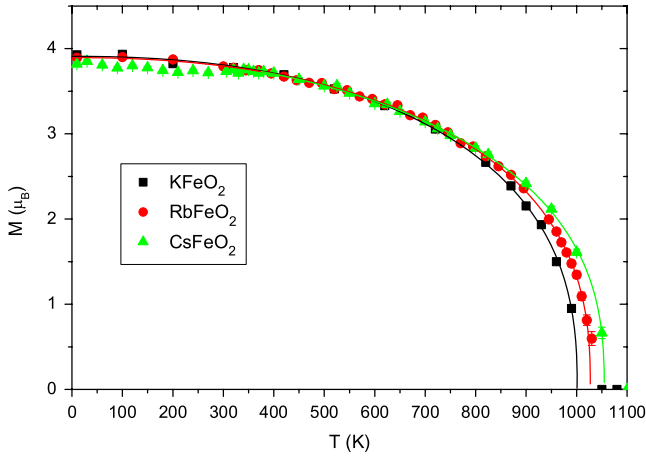


Figure 9. Temperature dependences of the refined magnetic Fe^{3+} magnetic moments for AFeO_2 (squares for $A = \text{K}$, circles for $A = \text{Rb}$, triangles for $A = \text{Cs}$) compounds. Solid lines are fits to the formula explained in the text. The peculiarity in the CsFeO_2 data at $T \approx 350$ K exactly coincides with the structural phase transition.

The data for CsFeO_2 were fitted only for $T > 350$ K, since the structural phase transition at ~ 350 K manifests itself by a peculiarity at this temperature, hence the precision of determination of the parameters α and M_0 is not very high for CsFeO_2 . The fitted Néel temperatures for the three AFeO_2 compounds amount to 1001(2) K, 1027(1) K and 1055(1) K for $A = \text{K}$, Rb , Cs , respectively. The estimated ‘critical exponent’ parameters β are very close in all three compounds: 0.382(16), 0.378(6) and 0.378(12) for $A = \text{K}$, Rb , Cs .

4. Discussion and conclusions

The structural and magnetic transitions in the AFeO_2 ($A = \text{K}$, Rb and Cs) compounds were investigated by neutron powder diffraction. The low-temperature and high-temperature modifications of all three compounds are isostructural to each other: the known KGaO_2 -type [2, 9–11] orthorhombic structure with $Pbca$ space group at low temperature and the cubic one with space group $Fd\bar{3}m$ at high temperature [2]. The lengths of the Fe-O bonds are very similar in all three compounds in both respective modifications, and remain almost constant at all temperatures, increasing on average only slightly—from ~ 1.86 Å at ~ 10 K to ~ 1.87 Å at ≥ 1000 K. The Fe-O-Fe bond angles, however, vary significantly, which is due to the different sizes of the A -cations—the more space needed to accommodate the A -cation, the more ‘straight’ (more close to 180°) the Fe-O-Fe bond angle. With increasing temperature, the Fe-O-Fe angles steadily increase, displaying observable discontinuities at the structural transition temperatures, which in turn leads to a discontinuous increase in the Fe-Fe separation with temperature. Upon heating through the structural transition points, the orientational long-range order of the Fe-O-Fe bindings is lost. The magnitudes of the Fe-O-Fe angles in these bindings are only slightly affected by the transitions, but their mutual orientations from one Fe-Fe junction to another most probably start varying dynamically in a collective manner, while they become no longer correlated

Table 3. Refined parameters of the fits of the data for the ordered magnetic moment values of the Fe^{3+} ions in AFeO_2 ($A = \text{K}$, Rb and Cs) to the formula (2).

Parameter	KFeO_2	RbFeO_2	CsFeO_2
M_0 (μ_B)	3.910 (18)	3.925 (9)	3.93 (3)
T_N (K)	1001 (2)	1027 (1)	1055 (1)
α	2.25 (13)	2.21 (5)	1.98 (13)
β	0.382 (16)	0.378 (6)	0.378 (12)

on a long-range scale. While the temperatures of the structural phase transitions differ significantly in the three studied compounds (~ 1003 , ~ 737 and ~ 350 K for $A = \text{K}$, Rb , Cs , see [2]), the magnetic transition temperatures are very close to each other (~ 1001 , ~ 1027 and ~ 1055 K respectively). The magnetic structures of all three compounds were determined to be antiferromagnetic with a low-temperature saturated value of the magnetic Fe^{3+} moments of $\sim 3.9 \mu_B$, and are characterized by antiferromagnetic Fe-Fe interactions in all four directions for each Fe ion. The observed value of $\sim 3.9 \mu_B$ of the low-temperature saturated magnetic Fe^{3+} moments is below the physically maximal expected value of $5 \mu_B$, probably because of the combination of the strong covalency effects between the magnetic 3d-orbitals of Fe and the 2p-orbitals of oxygen, leading to a reduction of the magnetic neutron scattering form factor of Fe , with transfer of magnetic moments to the oxygen ions, implying a net moment on the oxygen ions, see for example [12, 13], and of the defects in the magnetic structures. The direction of Fe^{3+} magnetic moments in KFeO_2 was found to be along the crystallographic b axis, in contrast to the previous finding of [4], and in RbFeO_2 and in CsFeO_2 along the crystallographic c axis.

Ideally it would be nice to find out the reasons for such close antiferromagnetic transition temperatures in these compounds, while the structural transitions occur at dramatically different temperatures. In the past, different phenomenological parameters were proposed in order to systematize the statistics on the Néel temperatures in the magnetic iron-based oxides, and even to predict them. Yet, having obtained the current newer results on the AFeO_2 ($A = \text{K}$, Rb and Cs) compounds, we fail to justify any of these.

For example, in [14], the T_N in RFeO_3 ($R = \text{rare earth}$) was found to be proportional to the average cosine of the Fe-O-Fe angles, ranging from ~ 630 to ~ 740 K for the $\cos(\text{Fe-O-Fe})$ changing from ~ 0.78 to ~ 0.92 . In our case, the observed values of $|\cos(\text{Fe-O-Fe})_{\text{orth}}|/|\cos(\text{Fe-O-Fe})_{\text{cub}}|$ obviously do not scale similarly to predict almost identical temperatures of the antiferromagnetic phase transitions. They amount to ~ 0.77 , ~ 0.84 and ~ 0.92 for $A = \text{K}$, Rb and Cs respectively at the antiferromagnetic transition temperatures; yet not only are the Néel temperatures very close to each other, but also they all fall completely out of the range predicted in [14] for the RFeO_3 compounds.

In [15], the value of T_c/n , where T_c is the antiferromagnetic transition temperature and n is the effective coordination number of Fe in different simple and mixed iron oxides, was found to be on average equal to 115 K (ranging from 106 to 132 K). In our study, again, this parameter (assuming the ideal

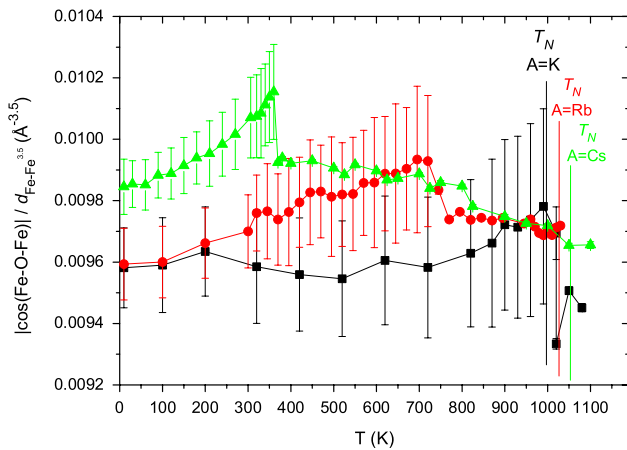


Figure 10. Temperature dependences of the $\frac{|\cos(M-O-M)|}{d_{M-O}^{3.5}}$ value for the $AFeO_2$ ($A = K, Rb$ and Cs) compounds.

four-fold coordination for Fe) would have to amount to ~ 250 , ~ 257 and ~ 264 K for $A = K, Rb$ and Cs respectively, thus falling far out of the predicted in [15] values.

Apart from the above mentioned empirical quantities, other possibilities have also been explored. For example in [16], for the case of the $RMnO_3$ manganites ($R =$ rare earth), a puzzling $T_N \sim \langle \cos^2 \phi \rangle$ proportionality has been established—which again is not consistent with our case.

Finally, in [17], the empirical proportionality of the exchange energy and of the magnetic transition temperatures to the $\frac{|\cos(M-O-M)|}{d_{M-O}^{3.5}}$ ratio, where $M-O$ is the metal–oxygen bond length, and $M-O-M$ is the valence angle for the case of the σ -bonding between the d-orbitals of metal and the p-orbitals of oxygen is discussed. In our case, this again would be incompatible if we take the $M-O$ bond lengths, yet there might be some kind of a universal scaling obtained if we take the $M-M$ bond lengths (Fe–Fe distances in our case) instead. The temperature dependences of the $\frac{|\cos(M-O-M)|}{d_{M-M}^{3.5}}$ values are presented in figure 10.

In a very recent publication [18], the origin of the high Néel temperatures in $KFeO_2$ and $RbFeO_2$ has been addressed by employing first-principles band-structure calculations and Monte-Carlo simulation. The authors were able to show that it is exactly the extremely short Fe–O bond lengths in the $KFeO_2$ and $RbFeO_2$ (significantly shorter than in various $AFeO_3$ oxides) which contribute to the much stronger covalency of these bonds, with exceptionally strong p–d hybridization producing the molecular bondlike states. Such highly localized states are claimed to be responsible for the unexpectedly strong superexchange interactions between the Fe ions and to lead to the exceptionally high values of T_N in the $KFeO_2$ and $RbFeO_2$ compounds. The predicted transition temperatures in [18] for

$KFeO_2$ and $RbFeO_2$ amount to 804 K and 821 K respectively, whereas our experimentally observed Néel temperatures have been found to be even higher— ~ 1001 K and ~ 1027 K respectively, and the one observed in $CsFeO_2$ (~ 1055 K) is herewith the highest ever observed in the Fe oxides.

When considering the obvious failures of previous concepts in rationalizing T_N , one must keep in mind that the systems under consideration here are rather unique because of the counteracting factors of influence (Fe–O–Fe angle and Fe–Fe distance) and also because the systems are dynamically disordered. This latter influence is hard to assess, thereby it also requires an independent probe for the structural and magnetic transformation with a different time resolution, namely Mössbauer spectroscopy [19].

Acknowledgments

This work is based on the experiments performed at the Swiss Spallation Neutron Source SINQ, Paul Scherrer Institut, Villigen, Switzerland.

References

- [1] Taylor D 1984 *Miner. Mag.* **48** 65–79
- [2] Ali N Z, Nuss J, Sheptyakov D and Jansen M 2010 *J. Solid State Chem.* **183** 752–9
- [3] Ichida T, Shinjo T, Bando Y and Takada T 1970 *J. Phys. Soc. Japan* **29** 1109–10
- [4] Tomkowicz Z and Szytuła A 1977 *J. Phys. Chem. Solids* **38** 1117–23
- [5] Trinschek D and Jansen M 1999 *Angew. Chem. Int. Edn* **38** 133–5
- [6] Fischer P *et al* 2000 *Physica B* **276** 146–7 <http://sinq.web.psi.ch/hrpt>
- [7] Wills A S 2000 *Physica B* **276** 680–1 Program available from www.ccp14.ac.uk
- [8] Rodríguez-Carvajal J 1993 *Physica B* **192** 55–69
- [9] Hoppe R 1965 *Angew. Chem. Int. Edn* **4** 534
- [10] Vielhaber E and Hoppe R 1969 *Z. Anorg. Allg. Chem.* **369** 14–32
- [11] Nuss J, Ali N Z and Jansen M 2007 *Acta Crystallogr. B* **63** 719–25
- [12] Byrom E, Freeman A J and Ellis D E 1975 *AIP Conf. Proc.* **24** 209–10
- [13] Tofield B C and Fender B E F 1970 *J. Phys. Chem Solids* **31** 2741–9
- [14] Treves D, Eibschitz M and Coppens P 1965 *Phys. Lett.* **18** 216–7
- [15] Gilleo M A 1958 *Phys. Rev.* **109** 777–81
- [16] Zhou J-S and Goodenough J B 2003 *Phys. Rev. B* **68** 054403
- [17] Harrison W A 1980 *Electronic Structure and the Properties of Solids* (San Francisco: Freeman)
- [18] Kim M, Kim B H, Choi H C and Min B I 2010 *Phys. Rev. B* **81** 212405
- [19] Ali N Z and Jansen M, paper in progress